MATERIALS SCIENCE

Formation of 2D and 3D multi-tori mesostructures via crystallization-driven self-assembly

Gerald Guerin[1,2]*, Menandro Cruz[2,3], Qing Yu[2]

The fabrication of three-dimensional (3D) objects by polymer self-assembly in solution is extremely challenging. Here, multi-tori mesostructures were obtained from the crystallization-driven self-assembly of a coil-crystalline block copolymer (BCP) in mixed solvents. The formation of these structures follows a multistep process. First, the BCP self-assembles into amorphous micrometer-large vesicles. Then, the BCP confined in these mesosized vesicles crystallizes. This second step leads to the formation of objects with shapes ranging from closed 3D multi-tori spherical shells to 2D toroid mesh monolayers, depending on the solvent mixture composition. This approach demonstrates how topological constraints induced by the specific interactions between coil-crystalline BCP and solvents can be used to prepare mesostructures of complex morphologies.

INTRODUCTION

In recent years, the study of the crystallization-driven self-assembly (CDSA) of coil-crystalline block copolymers (BCPs) in solution has become an important branch of polymer self-assembly. The living-like properties of CDSA demonstrated by Wang *et al.* (*1*) offer seemingly endless possibilities to generate structures of controlled size and morphology, opening the doors to the potential development of a multitude of devices (*2*–*5*). The main morphology reported was one-dimensional (1D), i.e., elongated homomicelles (*6*–*10*), as well as multi-block (*11*–*13*), patchy (*14*–*17*), and asymmetric comicelles (*18*, *19*). As the manipulation of 1D core-crystalline micelles became more common, sophisticated objects such as 2D (*20*–*22*), hybrid (*23*, *24*), and mesostructures (*25*, *26*) started to be presented.

The fabrication of isolated 3D mesoscale polymeric objects via bottom-up self-assembly, however, remains a daunting task. There are no compelling strategies that lead to the formation of 3D functional materials. The very few attempts to prepare these structures used preformed core-crystalline micelles as building blocks (*27*, *28*). This approach, however, failed to produce 3D mesostructures that persist in the solid state.

In the present work, we describe the successful preparation of 3D mesostructures as large as pollen grains (>10 μm). This unique type of structure was obtained by the CDSA of coil-crystalline BCPs in a mixture of solvents that are poor for both the coil and crystalline blocks. More specifically, we studied the self-assembly of polyferrocenyldimethylsilane-*block*-polystyrene (PFS_{26}-*b*-PS_{306}, with $M^{PS} \approx 30{,}000$) in an acetone/decane mixture containing 25 volume % of acetone, a composition where PFS_{26}-*b*-PS_{306} microphase separation is anticipated (*29*).

We show that the presence of PFS_{55}-*b*-PI_{500} (PI = polyisoprene) crystallites at an early stage of the self-assembly is essential for forming these micrometer large 3D multi-tori structures (Fig. 1 and fig. S1). Only perforated films could be observed when no PFS-*b*-PI seed micelles were present in the solution. We also show that the addition of an aliquot of a third solvent into the acetone/decane mixture strongly affects the morphology of final structure, either by greatly enhancing the sphericity of the multi-tori mesostructures or by inducing the formation of toroid mesh monolayers. Above all, the 3D multi-tori mesostructures have proven to be very stable at room temperature once transferred onto a substrate, preserving their morphology indefinitely, a prerequisite for the fabrication of 3D functional materials.

RESULTS

Preparation of multi-tori by self-assembly

The samples were prepared by quickly injecting a solution of PFS_{26}-*b*-PS_{306} in tetrahydrofuran (THF; 8 μl, $c = 10$ mg ml^{-1}) to 1 ml of a 25/75 (v/v%) acetone/decane mixture preheated at 35°C, and to which 20 μl of PFS_{55}-*b*-PI_{500} rod-like micelles in decane ($c = 0.2$ mg ml^{-1}) had been added (Fig. 1A). The solution was annealed for 1 hour and then cooled to room temperature. Within 1 hour after the heating was stopped, an aliquot of the solution was deposited on a transmission electron microscopy (TEM) grid at room temperature. The sample was finally imaged by scanning electron microscopy (SEM) and high-resolution TEM (HRTEM).

The protocol described above leads to the formation of a mixture of isolated toroids and open spherical multi-tori shells of ca. 20 μm diameter with a broad size distribution (Fig. 1, B to E). These shells look like broken or collapsed hollow spheres, consisting of toroids glued together. The toroids that compose the multi-tori appear to be relatively narrowly distributed in size (Fig. 1E), with an inner diameter close to 400 nm and an outer diameter of ca. 1 μm (because very few toroids lay flat on the TEM grid, the dimensions indicated are only semiquantitative).

It is worth noting that the multi-tori structures are unstable and collapse in on themselves when annealed at room temperature for a few extra hours in solution (fig. S2), but they preserve their morphology indefinitely once taken out of the solution (by depositing them on a TEM grid, for example). This allowed us to reimage the same TEM grid by SEM and HRTEM.

Intuitively, one would believe that the genesis of these massive objects is hierarchical and genuinely straightforward: First, PFS_{26}-*b*-PS_{306} toroids form by CDSA, and then, they are glued together by the remaining PFS_{26}-*b*-PS_{306} unimer in a sequence similar to that

[1]Shanghai Key Laboratory of Advanced Polymeric Materials, Key Laboratory for Ultrafine Materials of Ministry of Education, School of Materials Science and Engineering, East China University of Science and Technology, Shanghai 200237, China. [2]Department of Chemistry, University of Toronto, 80 St. George Street, Toronto, ON M5S 3H6, Canada. [3]Melville Laboratory for Polymer Synthesis, Department of Chemistry, University of Cambridge, Lensfield Road, Cambridge, UK.
*Corresponding author. Email: gguerin@ecust.edu.cn

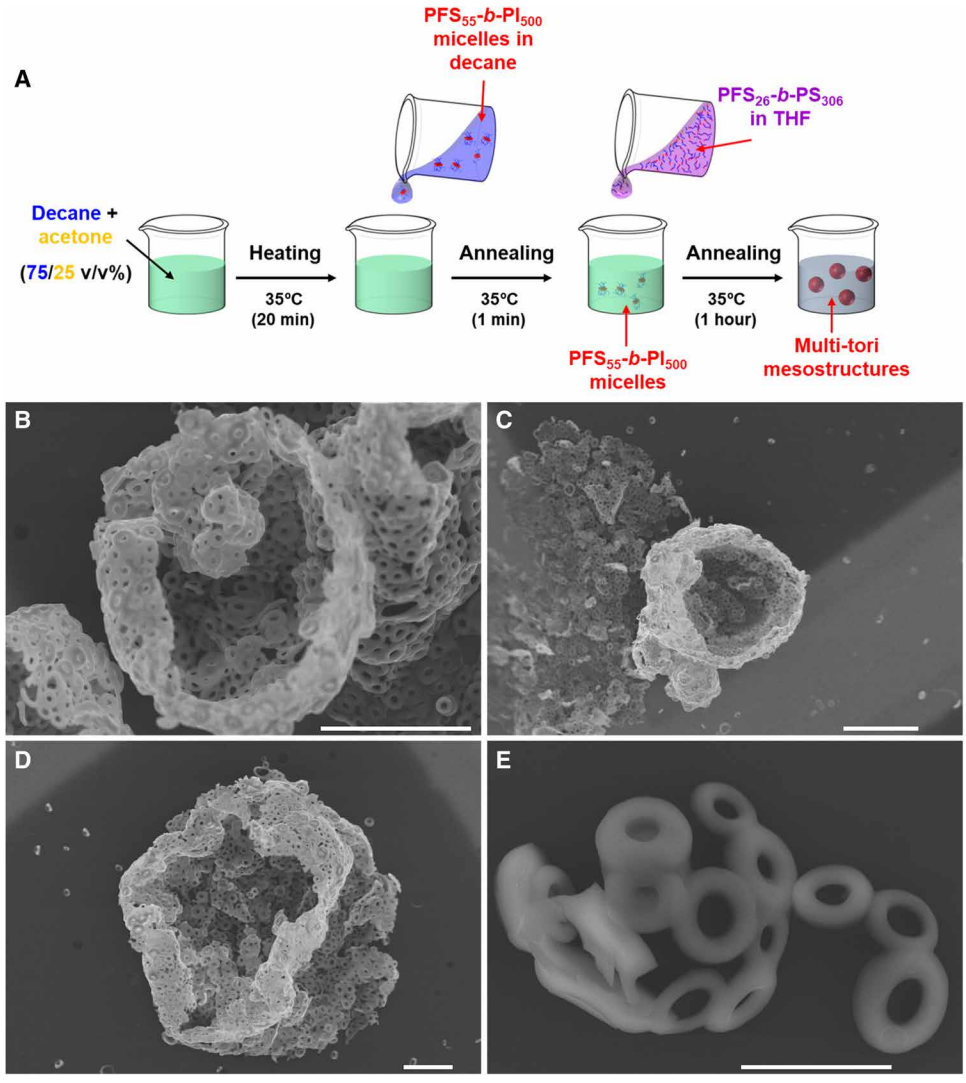

Fig. 1. Examples of 3D multi-tori mesostructures. (**A**) Protocol followed to prepare the multi-tori mesostructures. (**B** to **E**) Representative SEM micrographs of spherical hollow mesostructures consisting of a network of toroids. The structures were obtained by the self-assembly of PFS_{26}-*b*-PS_{306} in a mixture of 1.02 ml of acetone/decane (25/75, v/v%), containing 20 µl of PFS_{55}-*b*-PI_{500} core-crystalline elongated micelles ($c = 0.2$ mg ml^{-1}), and preheated at 35°C. An aliquot of PFS_{26}-*b*-PS_{306} dissolved in THF (8 µl, $c = 10$ mg ml^{-1}) was then injected, and the solution was annealed for 1 hour at 35°C and cooled to room temperature; TEM grids were prepared within 1 hour after heating. Scale bars, 10 µm (B to D) and 2 µm (E).

described by Cai *et al.* (*30*). These authors prepared sponge-like nanoporous superstructures using PFS_{48}-*b*-$[PMVS(OH)_2]_{326}$ BCP to glue already prepared PI_{1040}-*b*-$P2VP_{200}$ toroids.

We, thus, studied the sample by SEM at very short annealing times, i.e., 30 s and 5 min (Fig. 2 and fig. S3), hoping to capture images of isolated toroids, the expected building block and first step toward the formation of the 3D multi-tori structures. When we looked at the sample annealed for only 30 s (Fig. 2, A to C, and fig. S3, A to C), we were astonished to observe several large broken spherical shells of the size of the massive multi-tori structures and with a broad size distribution ranging from ca. 5 µm to more than 20 µm. The larger structures had a bumpy surface and appeared to have broken and flattened onto the TEM grid (Fig. 2, A and B), while the smaller structures were more raspberry-like, with bulges, or drupelets (to use a morphological analogy to raspberries), resembling the kippah micelles described by Azzam and Eisenberg (*31*) (Fig. 2C). In some cases, a hole located on the top of the drupelets is visible (Fig. 2C). After 5 min of annealing (Fig. 2, D to F, and fig. S3, D to F), the flattened structures are still observable, but they mainly consist of an assembly of a very large number of drupelets. The holes in the drupelets also appear to become wider as pointed out in Fig. 2F.

To further understand how these large vesicular mesostructures transformed into multi-tori, we performed a kinetic experiment and followed the evolution of these structures by TEM (Fig. 3). We prepared six vials containing a mixture of acetone/decane (25/75, v/v%) and the same amount of PFS_{55}-*b*-PI_{500} rod-like micelles. To each vial preheated at 35°C, we added a solution of PFS_{26}-*b*-PS_{306} in THF and annealed the solutions for different times. We took aliquots of the samples at 0.5, 5, 10, 20, 30, and 60 min and deposited them on TEM grids. For this experiment, we were particularly interested in studying the morphological evolution of the drupelets constituting

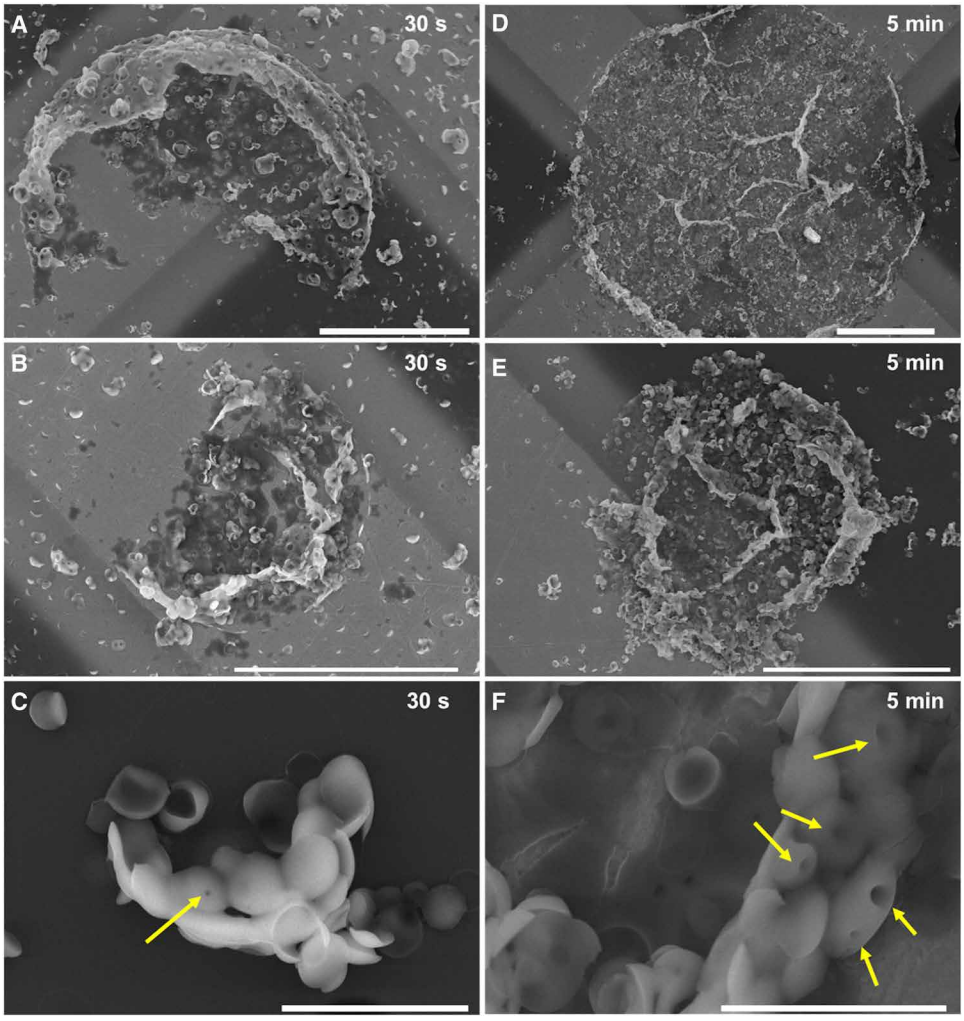

Fig. 2. SEM images of the 3D multi-tori mesostructures at short annealing times. Twenty microliters of a decane solution of PFS_{55}-*b*-PI_{500} seeds ($c = 0.2$ mg ml^{-1}) was added to 1 ml of acetone/decane mixture. The solution was then left to equilibrate at 35°C, and an aliquot of PFS_{26}-*b*-PS_{306} dissolved in THF (8 µl, $c = 10$ mg ml^{-1}) was injected. The solution was then annealed at 35°C. Samples were taken out from the solution and deposited on a TEM grid 30 s (**A** to **C**) and 5 min (**D** to **F**) after injection of PFS_{26}-*b*-PS_{306} unimer. The yellow arrows in (C) and (F) point at holes forming in the drupelets. Scale bars, 20 µm (A, B, D, and E) and 2 µm (C and F).

the mesostructures. HRTEM image of the sample annealed for 30 s (Fig. 3A and fig. S4, A and B) shows that, at this very short annealing time, the structures are made of what appears to be supramolecular assemblies of small spherical micelles.

After 5 min of annealing (Fig. 3B and fig. S4, C and D), the structures are still composed of small spherical micelles, but one can find, very occasionally, some curved elongated micelles as indicated by the arrows in Fig. 3B. When the sample was annealed for 10 min (Fig. 3, C and D, and fig. S4, E and F), the number as well as the length of the elongated micelles increased. These 1D micelles appear to be concentric and are present in every structure, along with a large amount of spherical micelles. At this stage, however, the concentric elongated micelles do not look like toroids. After 20 min of annealing (Fig. 3E and fig. S5, A and B), the vast majority of the spherical micelles have disappeared and have been replaced by concentric elongated micelles. Last, the toroids become clearly observable after 30 min of annealing (Fig. 3F and fig. S5, C and D). No obvious variation of the structures could be seen between 30 and 60 min of annealing (Fig. 3, F to H, and fig. S5, E and F).

Elongated micelles are typical of core-crystalline micelles obtained by CDSA of PFS BCPs. They were first reported by Massey *et al.* (*32*), who also demonstrated the role of PFS crystallization in the formation of these rod-like structures (*33*). Since then, a plethora of studies have confirmed the crucial role played by the crystallization of the PFS block in the formation of these 1D structures (*1*, *34*–*37*). We thus expected the concentric elongated micelles that assembled into toroids to have a crystalline core. To test this hypothesis, we studied a sample by x-ray diffraction (XRD). This experiment proved to be very challenging because we needed to prepare ca. 10 mg of product, while our usual experiments were performed with less than 0.1 mg. We first confirmed by SEM (fig. S6A) that the sample contained toroids, and we studied it by XRD. The XRD pattern is shown in fig. S6B. In addition to the very broad peaks centered at ca. $2\theta \approx 10°$ and $2\theta \approx 19°$ due to the amorphous halo of PS, we found a slightly broad peak centered at $2\theta \approx 13.7°$, corresponding to a *d*-spacing of 6.45 Å, typical of PFS core-crystalline micelles (*34*–*37*).

To ascertain the role of the PFS_{55}-*b*-PI_{500} seeds in the formation of the multi-tori structures, we injected a solution of PFS_{26}-*b*-PS_{306}

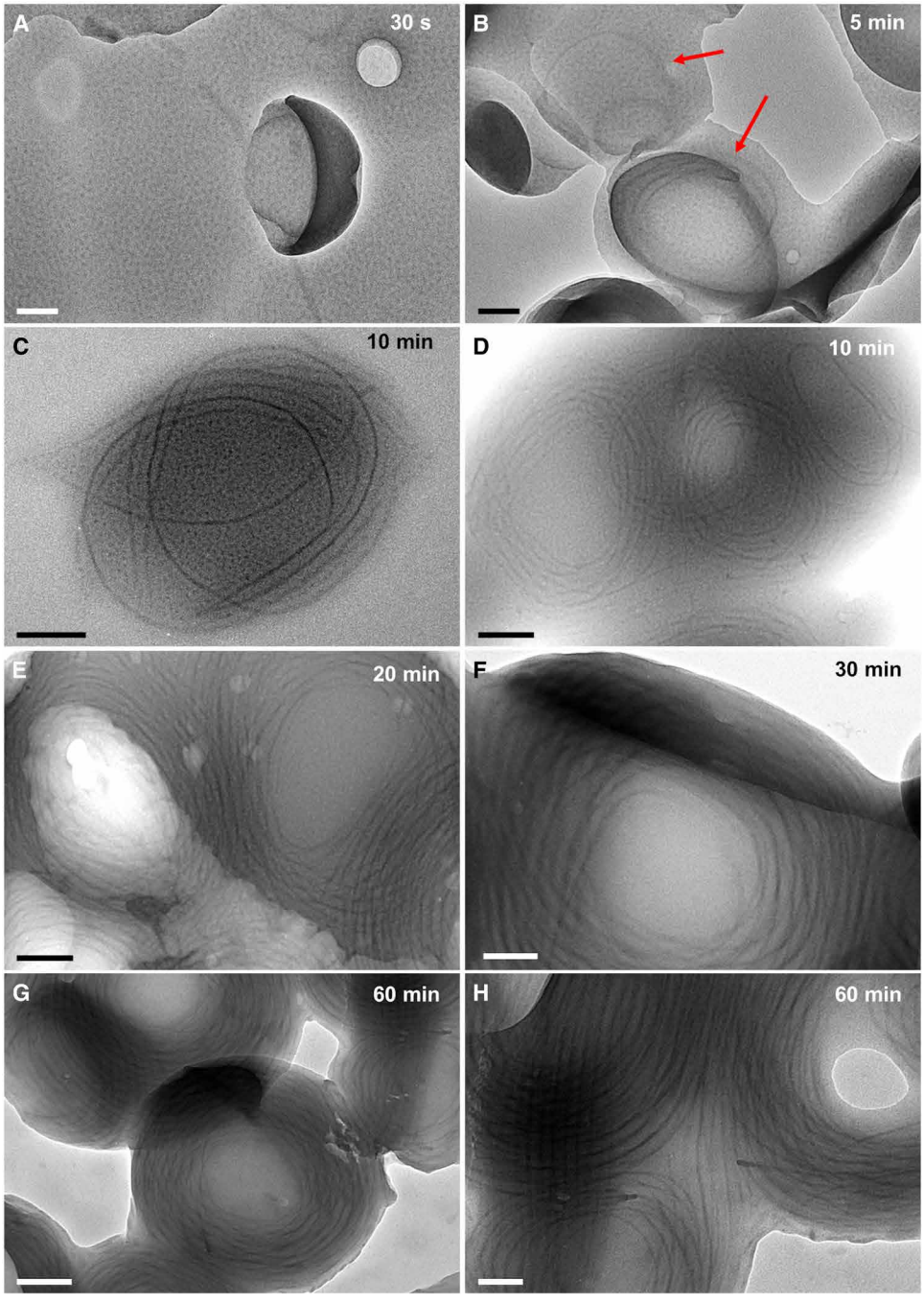

Fig. 3. Kinetic study of the formation of the toroids constituting the multi-tori mesostructures. Six vials were prepared. In each vial, 20 µl of a decane solution of PFS_{55}-*b*-PI_{500} seeds ($c = 0.2$ mg ml^{-1}) was added to 1 ml of acetone/decane mixture. The solution was then left to equilibrate at 35°C, and an aliquot of PFS_{26}-*b*-PS_{306} dissolved in THF (8 µl, $c = 10$ mg ml^{-1}) was injected. The solution was then annealed at 35°C. Samples were taken out from the solution and deposited on a TEM grid 30 s (**A**), 5 min (**B**), 10 min (**C** and **D**), 20 min (**E**), 30 min (**F**), and 1 hour (**G** and **H**) after injection of PFS_{26}-*b*-PS_{306} unimer. The red arrows in (B) point at the elongated micelles that started to appear in the drupelets after 5 min of annealing. Scale bars, 100 nm (A, B, F, and H) and 200 nm (C to E and G).

unimer in a decane/acetone mixture preheated at 35°C that did not contain any PFS_{55}-*b*-PI_{500} seeds. In the absence of PFS_{55}-*b*-PI_{500} micelles, we could not observe any multi-tori objects on the TEM grid, but only ill-defined perforated films (fig. S7A). A closer look at these structures by HRTEM (fig. S7, B to F) showed that they contain the spherical-like micelles that we observed at the early stage of the kinetics experiment (Fig. 3, A and B) along with a negligible number of elongated micelles (fig. S7F). This result confirmed that the crystallization of the PFS block is the driving force for the formation of the elongated micelles observed inside the toroids.

In a second control experiment, we postponed the addition of the PFS_{55}-*b*-PI_{500} seeds: We first injected the solution of PFS_{26}-*b*-PS_{306} unimer in the acetone/decane mixture, and we annealed the solution at 35°C for 1 hour before to add the PFS_{55}-*b*-PI_{500} seed solution. Just

after the addition of the seeds, we let the solution cool to room temperature, and after one extra hour of aging at room temperature, we studied the structures by SEM (fig. S8A) and HRTEM (fig. S8, B to F). Here again, we could only observe thick and smooth films that contained a large amount of spherical objects similar to those present at the early stage of the multi-tori formation (Fig. 3, A to C, and fig. S3) along with a relatively small number of straight elongated micelles. The occurrence of the elongated micelles was, however, more frequent than in the absence of PFS_{55}-*b*-PI_{500} seeds.

From these two control experiments, we infer that the PFS_{26}-*b*-PS_{306} vesicular mesostructure is a transient morphology. It gradually evolves with time to decrease the surface area between PFS_{26}-*b*-PS_{306} and the poor solvent mixture, leading to the formation of a thick film. The film is then too thick to confine micelle growth, and the usual rectilinear elongated micelles seeded by the late addition of the PFS_{55}-*b*-PI_{500} seeds are observed.

Additional information can also be obtained from SEM images of the edges of broken mesostructures (Fig. 4, A and B). When the structures fracture (either in solution or when deposited on the TEM grid), the crack appears to mostly propagate through the toroids and not between them. A high-magnification SEM image (Fig. 4B and fig. S9) of a fractured toroid shows the presence of the curved micelles in the toroid as well as what appears to be some micelles that are still bridging the two sections of the broken toroid. This result indicates that the connection between toroids is at least as strong as the toroids themselves. Another surprising finding is presented in Fig. 4D, where one clearly observes that the toroids are highly asymmetric, with a thickness of ca. 300 nm. They are flat on one side and inflated on the other, seemingly preserving the overall shape and orientation of the drupelets, as depicted in Fig. 4 (E and F).

The results presented in Figs. 2 to 4 disprove our intuitive rationale and show that the formation of these 3D mesostructures follows a unique pathway (Fig. 4, E and F). The first step consists of the supramolecular self-assembly of PFS_{26}-*b*-PS_{306} micelles with an amorphous core. The structures formed are micrometer large raspberry-like vesicles (Fig. 4E) with a broad size distribution. In the second step, the elongated core-crystalline PFS_{55}-*b*-PI_{500} micelles initiate

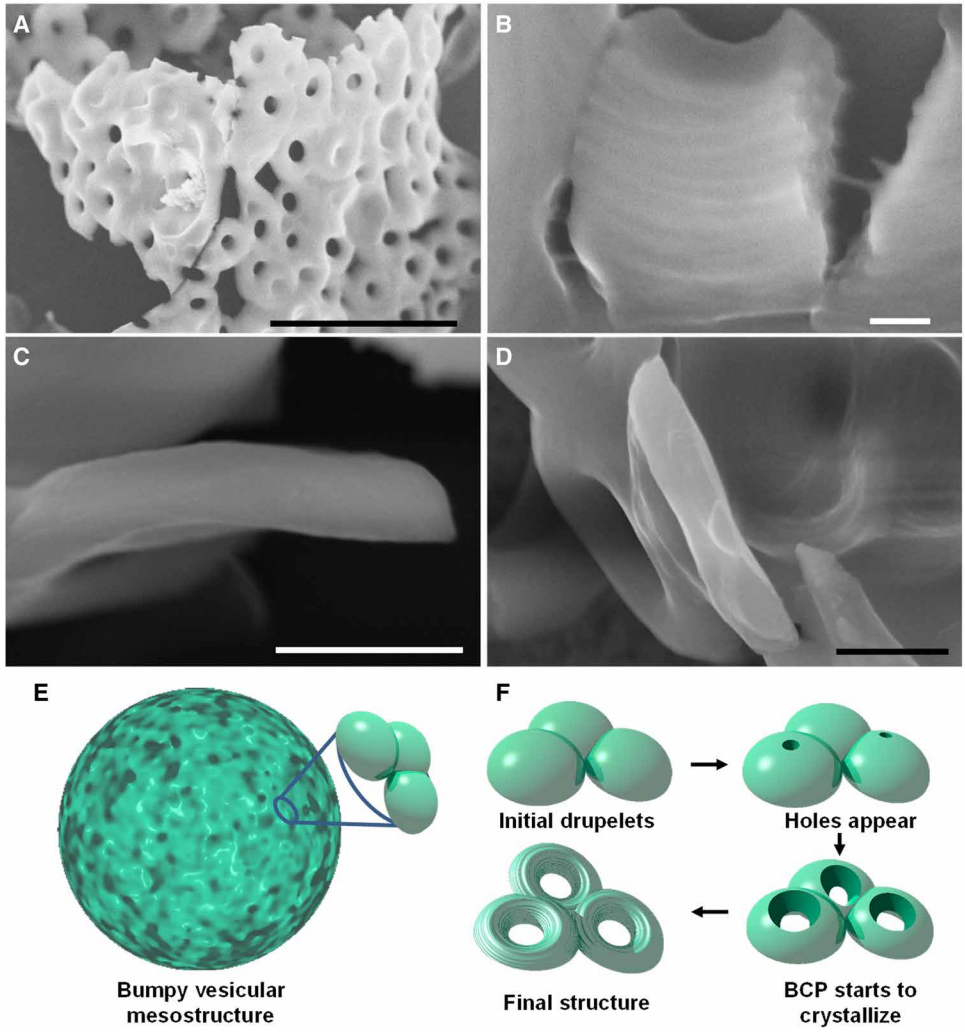

Fig. 4. Understanding the formation of the 3D multi-tori mesostructures. SEM micrographs of (**A**) the edge of a broken 3D multi-tori mesostructured, (**B**) a broken toroid, and (**C** and **D**) the side view of toroids of 3D multi-tori mesostructures. (**E**) Schematic representation of a micrometer large bumpy shell. (**F**) Schematic representation of the formation of the toroids. Scale bars, 5 μm (A and C), 100 nm (B), and 500 nm (D).

the crystallization of PFS_{26}-*b*-PS_{306} located in the drupelets (Fig. 4F), resulting in a sphere-to-cylinder morphology transition.

The sphere-to-cylinder transition of PFS micelles in polar solvents has been reported on several occasions (*37*–*40*), but it was unexpected in our system. In the present case, the morphology transition takes place in a confined environment, and we believe that the formation of the toroids is dictated by the raspberry-like topography of the thin vesicular mesostructures: As the PFS_{26}-*b*-PS_{306} elongated micelles extend, they follow the path with the smallest radius of curvature, growing parallel to the drupelet equatorial plane. As a consequence, the PFS_{26}-*b*-PS_{306} micelles grow in concentric rings and form toroids, as observed in Fig. 3 (E and F) and fig. S5 and as schematically represented in Fig. 4F.

The formation of these multi-tori shells is extremely sensitive to the ratio of acetone/decane used, as shown in figs. S10 and S11. These structures were only present for mixture compositions varying from 24 to 26 volume % of acetone (fig. S10). From 20 to 23 volume % (fig. S11, A to C), a mixture of toroids and 10–μm-long fibers (bundles of micelles) could be found on the TEM grids, while perforated films made of bundles of elongated micelles (fig. S11, D to F) were observed in the range of 27 to 30 volume % of acetone.

Cowie and McEwen (*29*) thoroughly studied the cosolvency effect of acetone/n-alkane binary mixtures on PS and showed that PS with a molecular weight (M_w) of 20 400 g mol^{-1} (close to that of the PS block used in this study) dissolves in acetone/decane mixtures ranging from ca. 60 to 95 volume % of acetone near room temperature. The unique self-assembly behavior presented here, however, occurs in a narrow range of solvent mixtures that is outside of the cosolvency window for the PS block (*29*). It is thus still unclear whether the self-assembly is directly related to the demixing of PFS_{26}-*b*-PS_{306} in the specific solvent mixture or whether the presence of the PFS block affects the range of the cosolvency window.

While the fractured 3D mesostructures shown in Fig. 1 are clearly hollow, they are not as spherical as represented in Fig. 4E, a consequence, we believe, of the rapid crystallization of PFS_{26}-*b*-PS_{306} in the drupelets, which would disrupt the roundness of the massive objects in solution. To slow down the crystallization and improve the sphericity of the mesostructures, we added 20 μl of methyl ethyl ketone (MEK), a better solvent for the PFS block, to the acetone/decane mixture, keeping the amount of acetone and decane unchanged. We then followed the same procedure as described previously, adding PFS_{55}-*b*-PI_{500} micelles and then PFS_{26}-*b*-PS_{306} at 35°C.

As shown in Fig. 5, the spherical structures formed in the presence of MEK were much better defined than those prepared in acetone/decane mixtures alone. For example, some closed or nearly closed structures could be observed on the TEM grid (Fig. 5, A and B, and fig. S12), which was not the case in acetone/decane mixtures. There is also little doubt that the opened structures shown in Fig. 5 (C and D) were 3D multi-tori mesospheres that subsequently fractured (fig. S13). The structures remained, however, broadly disperse in size, with diameters ranging from ca. 15 to 40 μm.

There have been several reports on the preparation of curved crystals by polymer crystallization at liquid/liquid interfaces. The most noticeable studies were reported by Li and co-workers (*41*–*44*), who prepared crystalsomes by crystallizing either polymers or BCPs at the interface of an oil-in-water miniemulsion. In the present case, such a mechanism would be relatively surprising because it requires a liquid/liquid phase separation in a solvent mixture (acetone/decane) that is normally miscible over all compositions and over a wide range of temperatures (*29*).

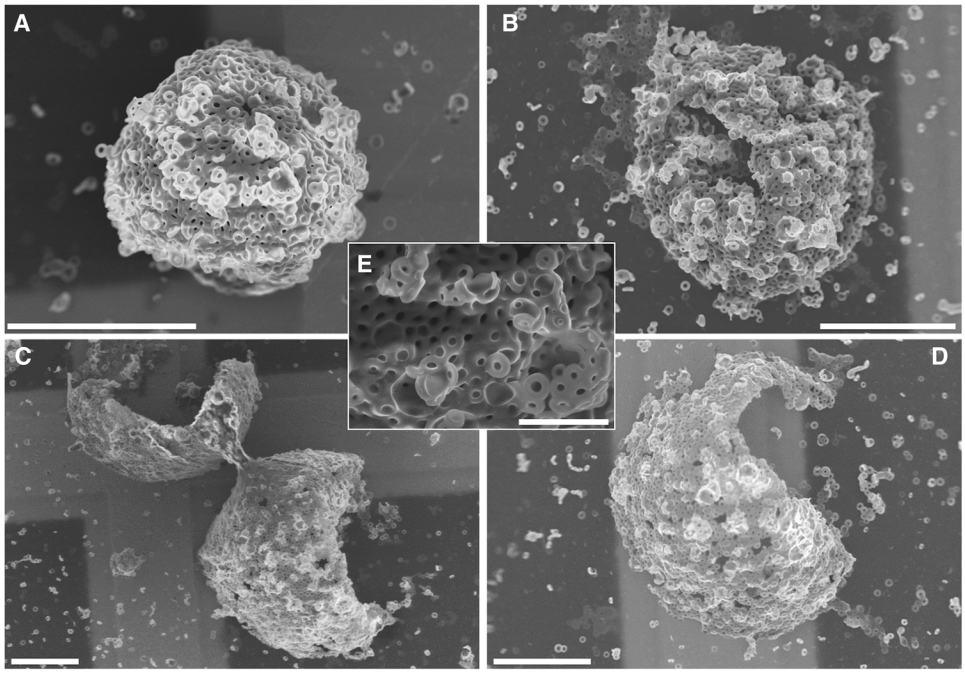

Fig. 5. Effect of an aliquot of MEK on the morphology of 3D multi-tori mesostructures. (**A** to **E**) Representative SEM micrographs of spherical hollow mesostructures consisting of a network of toroids. The mesostructures were prepared by adding 20 μl of MEK to a mixture of 1.02 ml of acetone/decane (25/75, v/v%), containing 20 μl of PFS_{55}-*b*-PI_{500} core-crystalline elongated micelles (c = 0.2 mg ml^{-1}). The solution was preheated at 35°C, and an aliquot of PFS_{26}-*b*-PS_{306} dissolved in THF (8 μl, c = 10 mg ml^{-1}) was injected. The solution was then annealed for 1 hour at 35°C and cooled to room temperature. TEM grids were prepared within 1 hour after heating. Scale bars, 20 μm (A to D) and 5 μm (E).

To test whether the presence of PFS_{26}-*b*-PS_{306} unimer could favor the formation of an emulsion-like suspension, we replaced MEK by a solvent that is miscible with acetone, but strongly immiscible with decane, to facilitate a possible microphase separation. Three solvents were tested: *N*,*N*-dimethylacetamide (DMAc) and *N*,*N*′-dimethylformamide (DMF), which are good solvents for PS, and acetonitrile (ACN), a poor solvent for PS. At first, we used DMAc, a good solvent for PS. Figure 6 (A to C) and fig. S14 show the structures obtained in the presence of 10 µl of DMAc. As anticipated, instead of the 3D mesostructures presented in Figs. 1 to 5, one observes very large objects of ill-defined shapes, with the long section ranging from 50 to 100 µm (Fig. 6A). Although the structures

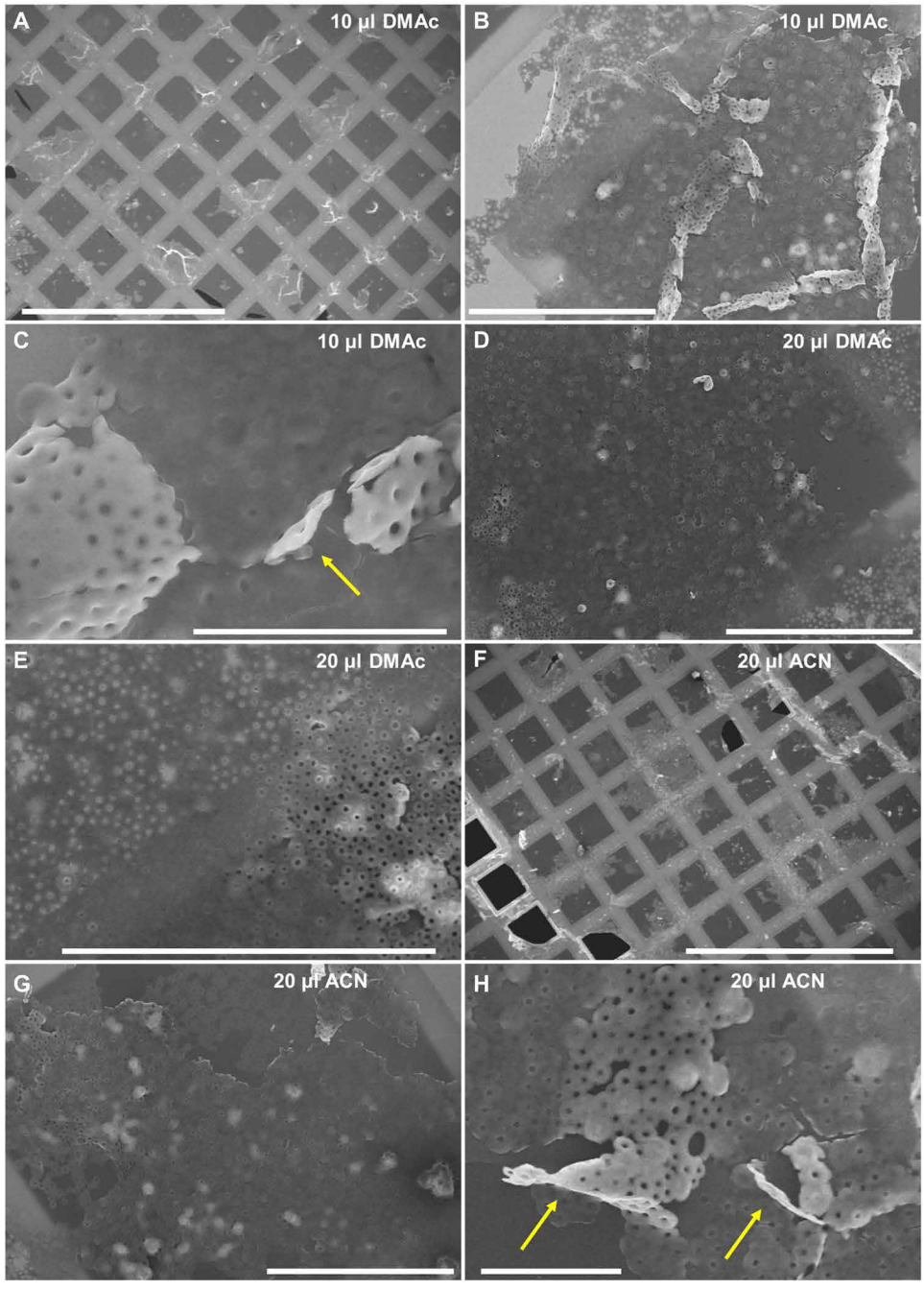

Fig. 6. Effect of an aliquot of DMAc and ACN on the morphology of multi-tori mesostructures. Representative SEM micrographs of mesostructures consisting of a network of toroids. The mesostructures were prepared by adding (**A** to **C**) 10 µl of DMAc, (**D** and **E**) 20 µl of DMAc, or (**F** to **H**) 20 µl of ACN to a mixture of 1.02 ml of acetone/decane (25/75, v/v%), containing 20 µl of PFS_{55}-*b*-PI_{500} core-crystalline elongated micelles ($c = 0.2$ mg ml^{-1}). The solution was preheated at 35°C, and an aliquot of PFS_{26}-*b*-PS_{306} dissolved in THF (8 µl, $c = 10$ mg ml^{-1}) was injected. The solution was then annealed for 1 hour at 35°C and cooled to room temperature. The yellow arrows in (C) and (H) point at sections of the monolayer perpendicular to the TEM grid and protruding toward the reader. TEM grids were prepared within 1 hour after heating. Scale bars, 500 µm (A and F), 40 µm (B, D, E, and G), and 10 µm (C and H).

deposited on the TEM grids have different morphologies, they all appear to be flat with ridges on their top, as one would expect from semirigid hollow objects collapsing onto a flat surface. A closer look at these structures (Fig. 6, B and C) confirms that they consist of a network of toroids. Similar structures could also be observed when 10 µl of DMF (fig. S15, A to C) was used, instead of DMAc. When ACN was used (fig. S15, D to F), SEM revealed the presence of broken sphere-like structures along with the flattened structures observed for DMAc and DMF. From these results, we conclude that the presence of a solvent immiscible with decane favored droplet coalescence to decrease the total surface area of the droplets.

To further increase droplet coalescence, we prepared solvent mixtures containing 20 µl of either DMAc (Fig. 6, D and E) or ACN (Fig. 6, F to H). This slight increase led to the formation of toroid mesh monolayers (Fig. 6, D to H, and fig. S16), as pointed out by the yellow arrows in Fig. 6 (C and H). These monolayers have a surface area of hundreds of square micrometers and a thickness corresponding to that of the toroids, i.e., around 300 nm, as evaluated from the images shown in Fig. 3 (C and D).

DISCUSSION

Here, we describe the preparation of 3D multi-tori structures via the CDSA of PFS_{26}-*b*-PS_{306} in a 25/75 (v/v%) acetone/decane mixture, triggered by the presence of core-crystalline PFS_{55}-*b*-PI_{500} elongated micelles. Both solvents are poor for each block. We show that these 3D structures are the result of a multistep process. In the first step, PFS_{26}-*b*-PS_{306} unimer self-assembles into micrometer-large raspberry-like vesicles. In the absence of core-crystalline micelles, the films remain mostly amorphous, but thicken with time, to give large perforated films.

In the presence of PFS_{55}-*b*-PI_{500} seed crystallites, the PFS_{26}-*b*-PS_{306} BCP inside the thin raspberry-like vesicles appears to quickly undergo a sphere-to-cylinder transition, leading to the formation of core-crystalline elongated micelles. Because of this short nucleation time, the seeded growth of the PFS_{26}-*b*-PS_{306} micelles is confined inside the wall of the vesicular mesostructures, and the elongated micelles are forced to grow concentrically along the equatorial plane of the drupelets, resulting in the formation of toroids. This mechanism is particularly remarkable and differs strongly from those previously reported in the literature (*45*, *46*).

The morphology of the multi-tori structures could also be tuned by adding an aliquot (10 or 20 µl) of a third solvent into the acetone/decane mixture. When MEK was used, the sphericity of the 3D objects was strongly increased, while 300-nm-thick toroid mesh monolayers could be obtained via the addition of a solvent immiscible with decane (DMAc, DMF, or ACN). These drastic changes in the final morphology of the multi-tori mesostructures induced by these subtle variations in solvent composition demonstrate the high potential of this approach to fabricate novel functional materials. It paves the way for new strategies to generate a plethora of intricate structures via bottom-up self-assembly.

MATERIALS AND METHODS

Materials

Decane (99+ %), THF (99+ %), acetone (99.9+ %), DMAc (99+ %), DMF (99+ %), and ACN (99.9+ %) were purchased from Sigma-Aldrich and used without further purification. PFS_{55}-*b*-PI_{500} (M_n = 48,200, Đ = 1.1) is the same sample reported in (*25*). PFS_{26}-*b*-PS_{306} (M_n = 40,600, PDI = 1.06) was synthesized in the group of I. Manners by anionic polymerization following established procedures (*47*).

SEM and HRTEM

SEM images were taken using a high-resolution Hitachi S-5200 instrument at a voltage of 5 kV. Samples were prepared by placing one drop of solution on a formvar-carbon–coated grid. The sample was left on the grid for few minutes (up to 5 min), and then the edge of the droplet was touched with a filter paper to remove excess liquid, allowing the grid to dry. The samples are very stable in the dry state; thus, the same grid could also be used for HRTEM imaging several months after they were deposited on the TEM grids. The HRTEM images were taken with a JEOL JEM-2100 instrument at an accelerating voltage of 200 kV.

TEM

TEM imaging of the PFS_{55}-*b*-PI_{500} core-crystalline micelles was performed on a Hitachi HT7700 TEM operating at an accelerating voltage of 80 kV. The TEM images were analyzed using the image processing program ImageJ.

Powder XRD experiments

Powder XRD experiments were performed on a Rigaku Ultima IV diffractometer at room temperature using Cu Kα radiation (λ = 1.5406 Å). The diffraction pattern was collected with an angular resolution of 0.02° per step and a scan speed of 1° per min.

Measurement of PFS_{55}-*b*-PI_{500} micelle length by TEM

To trigger the CDSA of the PFS_{26}-*b*-PS_{306}, we used a decane solution of core-crystalline micelles PFS_{55}-*b*-PI_{500} with an extremely broad length distribution. More than 700 micelles were measured by hand using the software ImageJ (National Institutes of Health, USA). The number and weight average length of the micelles, L_n and L_w, respectively, were calculated as

$$L_n = \frac{\sum_{i=1}^{N} N_i L_i}{\sum_{i=1}^{N} N_i} \qquad L_w = \frac{\sum_{i=1}^{N} N_i L_i^2}{\sum_{i=1}^{N} N_i L_i}$$

where N_i is the number of micelles of length L_i, and N is the total number of micelles examined. We found L_n = 530 nm, L_w = 1210 nm, and L_w/L_n = 2.3. The seed micelle solution contains a large majority of relatively short micelles (ca. 300 nm long), along with few micrometer-long micelles. A representative TEM image of these PFS_{55}-*b*-PI_{500} micelles, as well as their length distribution, is shown in fig. S17.

Preparation of 3D multi-tori mesostructures by self-assembly

The samples were prepared by injecting a solution of PFS_{26}-*b*-PS_{306} in THF (8 µl, c = 10 mg ml^{-1}) to 1 ml of a 25/75 (v/v%) acetone/decane mixture preheated at 35°C, and to which 20 µl of PFS_{55}-*b*-PI_{500} rod-like micelles in decane (c = 0.2 mg ml^{-1}) had been added. The solution was annealed for 1 hour and then cooled to room temperature. Within 1 hour after the heating was stopped, an aliquot of the solution was deposited on a TEM grid. The sample was finally imaged by SEM and HRTEM.

Preparation of mesostructures (i) in the absence of PFS_{55}-*b*-PI_{500} seeds and (ii) with a delayed addition of PFS_{55}-*b*-PI_{500} seeds

We annealed a PFS_{26}-*b*-PS_{306} unimer solution in acetone/decane for 1 hour at 35°C, in the absence of PFS_{55}-*b*-PI_{500} micelles. We then took out the solution to let it cool in air and split it in two vials (S_1 and S_2; 0.33 ml each). S_1 was aged for one additional hour at room temperature, while we added an aliquot (7 µl in decane) of a solution of PFS_{55}-*b*-PI_{500} micelles to S_2, just after it was taken out of the bath, and also let it age for one additional hour at room temperature. The samples were then examined by SEM and HRTEM.

An aliquot of the solution was deposited on a TEM grid held with an anti-capillary tweezer. The solution was left on the grid for 1 or 2 min, and excess solvent was removed by touching the side of the grid with a Kimwipe. The overall procedure took only few minutes, and we did not expect any preferential solvent evaporation that would affect the solvent ratio during this procedure. In addition, SEM imaging was performed on uncoated samples, which means that substantial height differences throughout the samples could lead to large differences in contrast due to charging effects.

Kinetic study of the formation of the 3D multi-tori mesostructures

The samples were prepared by injecting a solution of PFS_{26}-*b*-PS_{306} in THF (8 µl, c = 10 mg ml^{-1}) to six vials, each containing 1 ml of a 25/75 (v/v%) acetone/decane mixture preheated at 35°C, and to which 20 µl of PFS_{55}-*b*-PI_{500} rod-like micelles in decane (c = 0.2 mg ml^{-1}) had been added. At a given annealing time (namely, 0.5, 5, 10, 20, 30, and 60 min), an aliquot of the sample was taken out of the solution and deposited on the TEM grid. The excess of liquid was quickly removed with a filter paper. The two first samples (annealed for 30 s and 5 min) were imaged by SEM and HRTEM, and the four other samples were studied by HRTEM only.

Preparation of the sample for the XRD experiment

We injected 100 µl of a highly concentrated solution of PFS_{26}-*b*-PS_{306} in THF (c = 110 mg ml^{-1}) to 6 ml of a 25/75 (v/v%) acetone/decane mixture preheated at 35°C and containing 150 µl of PFS_{55}-*b*-PI_{500} seed crystallites dispersed in decane (c = 1 mg ml^{-1}). As soon as PFS_{26}-*b*-PS_{306} dissolved in THF was added, the solution became cloudy and a small amount precipitated out, most likely due to the high concentration of the unimer in THF. We thus transferred the cloudy solution in a second vial and annealed this vial for 1 hour at 35°C. The solution was then cooled to room temperature. After the sample was aged overnight, it fully precipitated out of the solution, settling down at the bottom of the vial. We then removed the solvent, verified by SEM that this specific protocol led to the formation of toroids, and performed XRD on the resulting powder. SEM imaging was performed with a Hitachi S-4800 instrument at a voltage of 3 kV. The sample was prepared by placing the powder onto a conducting tape.

Preparation of 3D multi-tori mesostructures in the presence of an aliquot of MEK

The mesostructures were prepared by adding 20 µl of MEK to a mixture of 1.02 ml of acetone/decane (25/75, v/v%), containing 20 µl of PFS_{55}-*b*-PI_{500} core-crystalline elongated micelles (c = 0.2 mg ml^{-1}). The solution was preheated at 35°C, and an aliquot of PFS_{26}-*b*-PS_{306} dissolved in THF (8 µl, c = 10 mg ml^{-1}) was injected. The solution was then annealed for 1 hour at 35°C and cooled to room temperature. TEM grids were prepared within 1 hour after heating.

Preparation of 2D toroid mesh monolayers in the presence of an aliquot of DMAc, DMF, or ACN

The mesostructures were prepared by adding 10 µl of DMAc to a mixture of 1.02 ml of acetone/decane (25/75, v/v%), containing 20 µl of PFS_{55}-*b*-PI_{500} core-crystalline elongated micelles (c = 0.2 mg ml^{-1}). The solution was preheated at 35°C, and an aliquot of PFS_{26}-*b*-PS_{306} dissolved in THF (8 µl, c = 10 mg ml^{-1}) was injected. The solution was then annealed for 1 hour at 35°C and cooled to room temperature. TEM grids were prepared within 1 hour after heating.

SUPPLEMENTARY MATERIALS

Supplementary material for this article is available at http://advances.sciencemag.org/cgi/content/full/6/16/eaaz7301/DC1

REFERENCES AND NOTES

1. X. Wang, G. Guerin, H. Wang, Y. Wang, I. Manners, M. A. Winnik, Cylindrical block copolymer micelles and co-micelles of controlled length and architecture. *Science* **317**, 644–647 (2007).
2. X.-H. Jin, M. B. Price, J. R. Finnegan, C. E. Boott, J. M. Richter, A. Rao, S. M. Menke, R. H. Friend, G. R. Whittell, I. Manners, Long-range exciton transport in conjugated polymer nanofibers prepared by seeded growth. *Science* **360**, 897–900 (2018).
3. J. Schöbel, M. Burgard, C. Hils, R. Dersch, M. Dulle, K. Volk, M. Karg, A. Greiner, H. Schmalz, Bottom-up meets top-down: Patchy hybrid nonwovens as an efficient catalysis platform. *Angew. Chem. Int. Ed.* **56**, 405–408 (2017).
4. M. C. Arno, M. Inam, Z. Coe, G. Cambridge, L. J. Macdougall, R. Keogh, A. P. Dove, R. K. O'Reilly, Precision epitaxy for aqueous 1D and 2D poly(ε-caprolactone) assemblies. *J. Am. Chem. Soc.* **139**, 16980–16985 (2017).
5. A. Nazemi, C. E. Boott, D. J. Lunn, J. Gwyther, D. W. Hayward, R. M. Richardson, M. A. Winnik, I. Manners, Monodisperse cylindrical micelles and block comicelles of controlled length in aqueous media. *J. Am. Chem. Soc.* **138**, 4484–4493 (2016).
6. M. Lazzari, M. A. López-Quintela, Micellization phenomena in semicrystalline block copolymers: Reflexive and critical views on the formation of cylindrical micelles. *Macromol. Rapid Commun.* **30**, 1785–1791 (2009).
7. G. Guérin, J. Raez, I. Manners, M. A. Winnik, Light scattering study of rigid, rodlike organometallic block copolymer micelles in dilute solution. *Macromolecules* **38**, 7819–7827 (2005).
8. N. Petzetakis, A. P. Dove, R. K. O'Reilly, Cylindrical micelles from the living crystallization-driven self-assembly of poly(lactide)-containing block copolymers. *Chem. Sci.* **2**, 955 (2011).
9. B. Fan, L. Liu, J.-H. Li, X.-X. Ke, J.-T. Xu, B.-Y. Du, Z.-Q. Fan, Crystallization-driven one-dimensional self-assembly of polyethylene-b-poly(tert-butylacrylate) diblock copolymers in DMF: Effects of crystallization temperature and the corona-forming block. *Soft Matter* **12**, 67–76 (2016).
10. U. Tritschler, J. Gwyther, R. L. Harniman, G. R. Whittell, M. A. Winnik, I. Manners, Toward uniform nanofibers with a π-conjugated core: Optimizing the "living" crystallization-driven self-assembly of diblock copolymers with a poly(3-octylthiophene) core-forming block. *Macromolecules* **51**, 5101–5113 (2018).
11. F. He, T. Gädt, I. Manners, M. A. Winnik, Fluorescent "barcode" multiblock co-micelles via the living self-assembly of di- and triblock copolymers with a crystalline core-forming metalloblock. *J. Am. Chem. Soc.* **133**, 9095–9103 (2011).
12. J. Qian, X. Li, D. J. Lunn, J. Gwyther, Z. M. Hudson, E. Kynaston, P. A. Rupar, M. A. Winnik, I. Manners, Uniform, high aspect ratio fiber-like micelles and block co-micelles with a crystalline π-conjugated polythiophene core by self-seeding. *J. Am. Chem. Soc.* **136**, 4121–4124 (2014).
13. G. Guerin, G. Cambridge, M. Soleimani, S. Mastour Tehrani, I. Manners, M. A. Winnik, Form factor of asymmetric elongated micelles: Playing with Russian dolls has never been so informative. *J. Phys. Chem. B* **118**, 10740–10749 (2014).
14. M. Cruz, J. Xu, Q. Yu, G. Guerin, I. Manners, M. A. Winnik, Visualizing nanoscale coronal segregation in rod-like micelles formed by co-assembly of binary block copolymer blends. *Macromol. Rapid Commun.* **39**, e1800397 (2018).
15. J. Xu, H. Zhou, Q. Yu, I. Manners, M. A. Winnik, Competitive self-assembly kinetics as a route to control the morphology of core-crystalline cylindrical micelles. *J. Am. Chem. Soc.* **140**, 2619–2628 (2018).
16. S. Rosenfeldt, F. Lüdel, C. Schulreich, T. Hellweg, A. Radulescu, J. Schmelz, H. Schmalz, L. Harnau, Patchy worm-like micelles: Solution structure studied by small-angle neutron scattering. *Phys. Chem. Chem. Phys.* **14**, 12750–12756 (2012).

17. A. M. Oliver, J. Gwyther, M. A. Winnik, I. Manners, Cylindrical Micelles with "patchy" coronas from the crystallization-driven self-assembly of ABC triblock terpolymers with a crystallizable central polyferrocenyldimethylsilane segment. *Macromolecules* **51**, 222–231 (2018).
18. P. A. Rupar, L. Chabanne, M. A. Winnik, I. Manners, Non-centrosymmetric cylindrical micelles by unidirectional growth. *Science* **337**, 559–562 (2012).
19. Z. M. Hudson, C. E. Boott, M. E. Robinson, P. A. Rupar, M. A. Winnik, I. Manners, Tailored hierarchical micelle architectures using living crystallization-driven self-assembly in two dimensions. *Nat. Chem.* **6**, 893–898 (2014).
20. H. Qiu, Y. Gao, C. E. Boott, O. E. C. Gould, R. L. Harniman, M. J. Miles, S. E. D. Webb, M. A. Winnik, I. Manners, Uniform patchy and hollow rectangular platelet micelles from crystallizable polymer blends. *Science* **352**, 697–701 (2016).
21. A. Nazemi, X. He, L. R. MacFarlane, R. L. Harniman, M.-S. Hsiao, M. A. Winnik, C. F. J. Faul, I. Manners, Uniform "patchy" platelets by seeded heteroepitaxial growth of crystallizable polymer blends in two dimensions. *J. Am. Chem. Soc.* **139**, 4409–4417 (2017).
22. X. He, M.-S. Hsiao, C. E. Boott, R. L. Harniman, A. Nazemi, X. Li, M. A. Winnik, I. Manners, Two-dimensional assemblies from crystallizable homopolymers with charged termini. *Nat. Mater.* **16**, 481–488 (2017).
23. L. Jia, G. Zhao, W. Shi, N. Coombs, I. Gourevich, G. C. Walker, G. Guerin, I. Manners, M. A. Winnik, A design strategy for the hierarchical fabrication of colloidal hybrid mesostructures. *Nat. Commun.* **5**, 3882 (2014).
24. L. Jia, A. Petretic, G. Molev, G. Guerin, I. Manners, M. A. Winnik, Hierarchical Polymer–carbon nanotube hybrid mesostructures by crystallization-driven self-assembly. *ACS Nano* **9**, 10673–10685 (2015).
25. L. Jia, G. Guerin, Y. Lu, Q. Yu, I. Manners, M. A. Winnik, Creating biomorphic barbed and branched mesostructures in solution through block copolymer crystallization. *Angew. Chem. Int. Ed. Engl.* **57**, 17205–17210 (2018).
26. X. Li, Y. Gao, C. E. Boott, D. W. Hayward, R. Harniman, G. R. Whittell, R. M. Richardson, M. A. Winnik, I. Manners, "Cross" supermicelles via the hierarchical assembly of amphiphilic cylindrical triblock comicelles. *J. Am. Chem. Soc.* **138**, 4087–4095 (2016).
27. L. Jia, L. Tong, Y. Liang, A. Petretic, G. Guerin, I. Manners, M. A. Winnik, Templated fabrication of fiber-basket polymersomes via crystallization-driven block copolymer self-assembly. *J. Am. Chem. Soc.* **136**, 16676–16682 (2014).
28. H. Dou, M. Li, Y. Qiao, R. Harniman, X. Li, C. E. Boott, S. Mann, I. Manners, Higher-order assembly of crystalline cylindrical micelles into membrane-extendable colloidosomes. *Nat. Commun.* **8**, 426 (2017).
29. J. M. G. Cowie, I. J. McEwen, Polymer-cosolvent systems: 6. Phase behaviour of polystyrene in binary mixed solvents of acetone with n-alkanes-examples of 'classic cosolvency'. *Polymer* **24**, 1449–1452 (1983).
30. J. Cai, K. P. Mineart, X. Li, R. J. Spontak, I. Manners, H. Qiu, Hierarchical self-assembly of toroidal micelles into multidimensional nanoporous superstructures. *ACS Macro Lett.* **7**, 1040–1045 (2018).
31. T. Azzam, A. Eisenberg, Fully collapsed (Kippah) vesicles: Preparation and characterization. *Langmuir* **26**, 10513–10523 (2010).
32. J. Massey, K. N. Power, I. Manners, M. A. Winnik, Self-assembly of a novel organometallic–inorganic block copolymer in solution and the solid state: Nonintrusive observation of novel wormlike poly(ferrocenyldimethylsilane)-*b*-poly(dimethylsiloxane) micelles. *J. Am. Chem. Soc.* **120**, 9533–9540 (1998).
33. J. A. Massey, K. Temple, L. Cao, Y. Rharbi, J. Raez, M. A. Winnik, I. Manners, Self-assembly of organometallic block copolymers: The role of crystallinity of the core-forming polyferrocene block in the micellar morphologies formed by poly(ferrocenylsilane-*b*-dimethylsiloxane) in *n*-alkane solvents. *J. Am. Chem. Soc.* **122**, 11577–11584 (2000).
34. F. Qi, G. Guerin, G. Cambridge, W. Xu, I. Manners, M. A. Winnik, Influence of solvent polarity on the self-assembly of the crystalline–coil diblock copolymer polyferrocenylsilane-*b*-polyisoprene. *Macromolecules* **44**, 6136–6144 (2011).
35. J. B. Gilroy, T. Gädt, G. Whittell, L. Chabanne, J. M. Mitchels, R. M. Richardson, M. A. Winnik, I. Manners, Monodisperse cylindrical micelles by crystallization-driven living self-assembly. *Nat. Chem.* **2**, 566–570 (2010).
36. J. B. Gilroy, P. A. Rupar, G. R. Whittell, L. Chabanne, N. J. Terrill, M. A. Winnik, I. Manners, R. M. Richardson, Probing the structure of the crystalline core of field-aligned, monodisperse, cylindrical polyisoprene-block-polyferrocenylsilane micelles in solution using synchrotron small- and wide-angle x-ray scattering. *J. Am. Chem. Soc.* **133**, 17056–17062 (2011).
37. L. Shen, H. Wang, G. Guerin, C. Wu, I. Manners, M. A. Winnik, A micellar sphere-to-cylinder transition of poly(ferrocenyldimethylsilane-*b*-2-vinylpyridine) in a selective solvent driven by crystallization. *Macromolecules* **41**, 4380–4389 (2008).
38. S. F. Mohd Yusoff, M.-S. Hsiao, F. H. Schacher, M. A. Winnik, I. Manners, Formation of lenticular platelet micelles via the interplay of crystallization and chain stretching: Solution self-assembly of poly(ferrocenyldimethylsilane)-*block*-poly(2-vinylpyridine) with a crystallizable core-forming metalloblock. *Macromolecules* **45**, 3883–3891 (2012).
39. M.-S. Hsiao, S. F. M. Yusoff, M. A. Winnik, I. Manners, Crystallization-driven self-assembly of block copolymers with a short crystallizable core-forming segment: Controlling micelle morphology through the influence of molar mass and solvent selectivity. *Macromolecules* **47**, 2361–2372 (2014).
40. H. Zhou, Y. Lu, M. Zhang, G. Guerin, I. Manners, M. A. Winnik, PFS-*b*-PNIPAM: A first step toward polymeric nanofibrillar hydrogels based on uniform fiber-like micelles. *Macromolecules* **49**, 4265–4276 (2016).
41. W. Wang, H. Qi, T. Zhou, S. Mei, L. Han, T. Higuchi, H. Jinnai, C. Y. Li, Highly robust crystalsome via directed polymer crystallization at curved liquid/liquid interface. *Nat. Commun.* **7**, 10599 (2016).
42. W. Wang, M. C. Staub, T. Zhou, D. M. Smith, H. Qi, E. D. Laird, S. Cheng, C. Y. Li, Polyethylene nano crystalsomes formed at a curved liquid/liquid interface. *Nanoscale* **10**, 268–276 (2017).
43. H. Qi, H. Zhou, Q. Tang, J. Y. Lee, Z. Fan, S. Kim, M. C. Staub, T. Zhou, S. Mei, L. Han, D. J. Pochan, H. Cheng, W. Hu, C. Y. Li, Block copolymer crystalsomes with an ultrathin shell to extend blood circulation time. *Nat. Commun.* **9**, 3005 (2018).
44. M. C. Staub, C. Y. Li, Confined and directed polymer crystallization at curved liquid/liquid interface. *Macromol. Chem. Phys.* **219**, 1700455 (2018).
45. H. Qiu, A. M. Oliver, J. Gwyther, J. Cai, R. L. Harniman, D. W. Hayward, I. Manners, Uniform toroidal micelles via the solution self-assembly of block copolymer–homopolymer blends using a "frustrated crystallization" approach. *Macromolecules* **52**, 113–120 (2019).
46. D. Presa-Soto, G. A. Carriedo, R. de la Campa, A. Presa Soto, Formation and reversible morphological transition of bicontinuous nanospheres and toroidal micelles by the self-assembly of a crystalline-*b*-coil diblock copolymer. *Angew. Chem. Int. Ed.* **55**, 10102–10107 (2016).
47. Y. Ni, R. Rulkens, I. Manners, Transition metal-based polymers with controlled architectures: Well-defined poly(ferrocenylsilane) homopolymers and multiblock copolymers via the living anionic ring-opening polymerization of silicon-bridged [1] ferrocenophanes. *J. Am. Chem. Soc.* **118**, 4102–4114 (1996).

Acknowledgments: The Toronto authors thank NSERC Canada for financial support. G.G. thanks M. A. Winnik for very helpful comments and suggestions and L. Zhou at the Research Center of Analysis and Test of East China University of Science and Technology for help on TEM imaging. G.G. and Q.Y. also thank I. Manners for providing the access of his laboratory for the synthesis of the PFS polymers. **Funding:** M.C. and Q.Y. were supported by NSERC Canada grant RGPIN-2017-03741. **Author contributions:** G.G. conceived the project, performed the experiments, and wrote the manuscript. M.C. designed and performed some experiments. Q.Y. synthesized the polymers. G.G. prepared the manuscript. The whole project was supervised by G.G. **Competing interests:** The authors declare that they have no competing interests. **Data and materials availability:** All data needed to evaluate the conclusions in the paper are present in the paper and/or the Supplementary Materials. Additional data related to this paper may be requested from the authors.

Submitted 3 October 2019
Accepted 22 January 2020
Published 15 April 2020
10.1126/sciadv.aaz7301

Citation: G. Guerin, M. Cruz, Q. Yu, Formation of 2D and 3D multi-tori mesostructures via crystallization-driven self-assembly. *Sci. Adv.* **6**, eaaz7301 (2020).